ELSEVIER

### Contents lists available at ScienceDirect

# Scripta Materialia

journal homepage: www.elsevier.com/locate/scriptamat



# Dynamic recovery observed in distinct grains within a polycrystalline nickel-based superalloy during cyclic high temperature fatigue via high energy X-ray diffraction microscopy



Sven E. Gustafson<sup>a</sup>, Darren C. Pagan<sup>b</sup>, Paul A. Shade<sup>c</sup>, Michael D. Sangid<sup>a,\*</sup>

- <sup>a</sup> School of Aeronautics and Astronautics, Purdue University, 701 W. Stadium Ave, West Lafayette, IN 47906, USA
- <sup>b</sup> Cornell High Energy Synchrotron Source, Ithaca, NY, USA
- <sup>c</sup> Materials and Manufacturing Directorate, Air Force Research Laboratory, Wright-Patterson AFB, OH 45433, USA

#### ARTICLE INFO

# Article history: Received 15 July 2020 Revised 19 September 2020 Accepted 2 October 2020 Available online 12 October 2020

Keywords: Thermomechanical fatigue Microstructure X-ray diffraction Recovery Synchrotron radiation

#### ABSTRACT

Elastic micromechanical fields are tracked for a nickel-based superalloy polycrystal via high energy X-ray diffraction microscopy (HEDM) and corresponding intragranular deformation metrics are determined with peak broadening analysis during cyclic high temperature loading. A low solvus, high refractory (LSHR) sample with 252 grains was subjected to uniaxial tension and held under fixed displacement while thermally cycling between 460  $^{\circ}$ C and 770  $^{\circ}$ C with intermittent HEDM characterization to study the grain average response to thermo-mechanical deformation. Elevated temperatures were found to allow for heterogeneous amounts of recovery amongst distinct grains within the sampled region, indicating complex grain interactions; the extent of recovery was greater at higher temperatures.

© 2020 Acta Materialia Inc. Published by Elsevier Ltd. All rights reserved.

Nickel-based superalloys have been critical in the advancement of gas turbine engines, due to their ability to maintain strength at elevated temperatures. Components in these hot engine sections undergo thermo-mechanical fatigue (TMF) and thus have complex failure mechanisms that depend heavily on temperature, strain rate, strain range, and strain-temperature phasing [1]. Life prediction models have been designed from a combination of specimenlevel testing and post-mortem fractography [2-4]. As such, current failure predictions are informed by conservative design practices to ensure safety, which can lead to premature removal of components from service and associated increased costs. Fatigue life scatter can be attributed to variability in the microstructure of the material [5], yet, due to the historical sparse availability of grain scale data during TMF loading, efforts to explore the microstructural impact on TMF has been limited [6]. Additional in-situ data during TMF experiments on the grain and sub-grain scales are needed to allow for the full interrogation of microstructural events acting on these length scales.

One TMF related microstructural phenomenon in metals is recovery, which occurs during the processing of components (such as annealing) and is often accompanied by recrystallization. In re-

E-mail address: msangid@purdue.edu (M.D. Sangid).

covery, grains rearrange defects in their crystals' structure to reduce their stored energy. Further, dynamic recovery occurs during loading and is known to cause a reduction in the flow stress of a material, especially at higher temperatures [7]. Upon large deformations, dislocations can arrange into dislocation cell structures leading to long range stresses within grains [8,9]. Dislocation rearrangement and cell structure formation are accelerated at elevated temperatures, and as such, dynamic recovery is most often seen under this condition. Classically, the recovery process has been split into three stages, rapid annihilation of dislocations within cell interiors, cell walls tightening into sharp sub-grain boundaries, and sub-grain coarsening [10,11]. The initial two stages have been combined in the past; however, the first stage is a continuation of unloading effects and occurs within minutes while the tightening of cell walls can take longer (often hours depending on temperature) and is responsible for a reduction in flow stress [11]. Further complicating the effects of dynamic recovery, nickel-based superalloys are unique from many other material systems due to a coherent  $\gamma'$ precipitate phase, which resides within the  $\gamma$  matrix, and serves to improve the high temperature creep performance of the material. In some materials, this dynamic recovery process is seen to increase fatigue life performance at higher temperatures [1]; however, at elevated temperatures the  $\gamma^\prime$  precipitate phase in nickelbased superalloys begins to coarsen, reducing its creep resistance and therefore the fatigue performance [2].

<sup>\*</sup> Corresponding author: 701 W. Stadium Ave. West Lafayette, IN 47907-2045, USA.

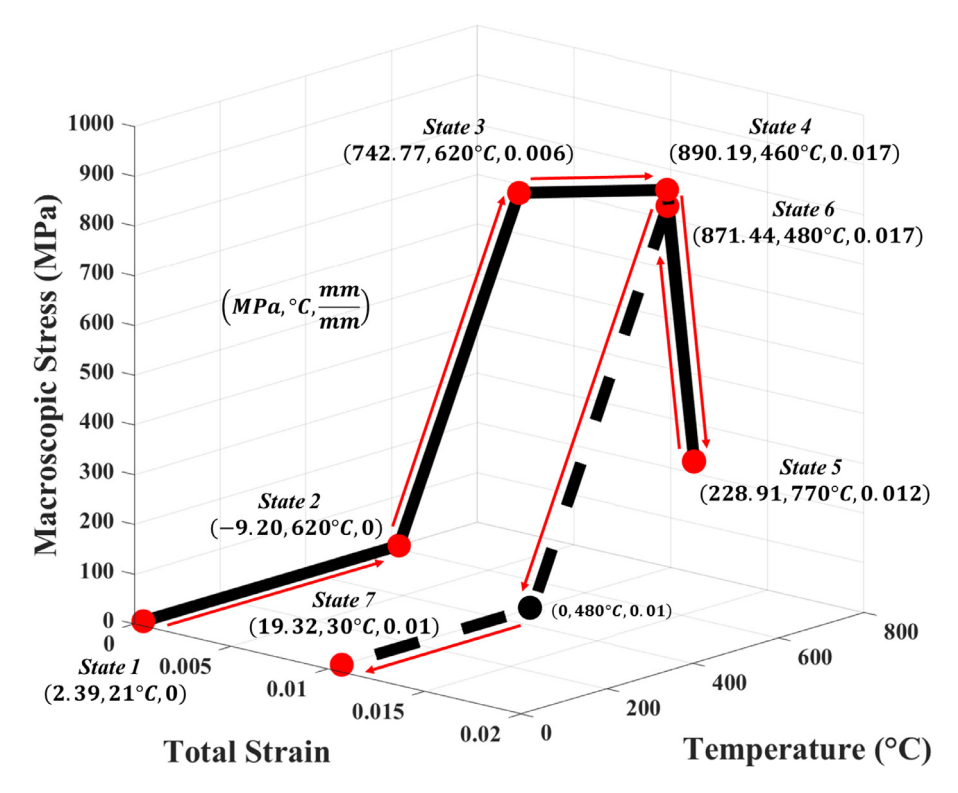


Fig. 1. Loading schematic followed during HEDM experiment.

Classically, many dynamic recovery studies have been performed on single crystals characterized by transmission electron microscopy, as larger scale, 3D non-destructive techniques to investigate dynamic recovery were not available. Advancements have been made in the X-ray community to allow for sub-grain information to be investigated during deformation [12], as well as during the recovery and recrystallization process [13]. Over the past decade, complementary techniques, such as high energy Xray diffraction microscopy (HEDM), have allowed for the interrogation of grain averaged statistics during in-situ mechanical loading [14] and external environments have been added to allow for the combination of thermal and mechanical loading during characterization [15]. The current study builds the framework for conducting strain-temperature phasing TMF during X-ray interrogation with a non-destructive analysis of dynamic recovery in a polycrystalline sample during in-situ high temperature cyclic loading via HEDM and peak broadening analysis. This letter investigates the impact of (i) grain-scale elastic (stress) statistics via HEDM and (ii) plasticity metrics via peak broadening analysis, on dynamic recovery within grains, and provides the context necessary to probe the failure mechanisms governing components which undergo TMF loading conditions.

The material used in this study was LSHR (low solvus, high refractory) and its general properties, composition, and thermal characteristics are detailed by Gabb et al. [16]. The particular processing procedure began with an isothermal forging and was followed by a 1-hour supersolvus heating at 1171 °C. Next, the material was heat treated at 855 °C for 4 h, then at 775 °C for 8 h, and finally cooled in air to achieve the desired precipitate structure [17]. A rotational and axial motion system (RAMS2) [18] was coupled with a halogen bulb furnace [15] to facilitate the required TMF loading (with approximately  $\pm 10$  °C control) using displacement control under the spatial and rotational restrictions of a general X-ray diffraction setup. HEDM analysis was conducted during seven distinct, interrupted loading states as shown as red dots in

Fig. 1. The sample, which was electrical discharge machined to the final 29 mm height, had a gauge length of 1.5 mm and square cross section of approximately  $1 \, mm^2$  (Fig. 2a). The study began at state 1 with both a near-field HEDM (NF-HEDM) scan [19] and a far-field HEDM (FF-HEDM) scan [20,21] in a nominally unloaded, room temperature configuration. In each of the following states, only a FF-HEDM scan was taken to track the grain averaged elastic strains. The sample was heated, under load control at nominally zero macroscopic load, to 620 °C for state 2. In state 3, a macroscopic stress of 742.77  $\pm$  0.03 MPa was applied, which is close to the macroscopic yield of the material as determined from prior mechanical testing. For states 4-6, the sample was cycled between 460 °C, 770 °C, and 480 °C while in displacement control, which resulted in 890.19  $\pm$  0.03 MPa, 228.91  $\pm$  0.06 MPa, and  $871.44 \pm 0.6$  MPa macroscopic values of stress upon the sample, respectively. Finally, in state 7, the sample was unloaded and brought to nominally room temperature where a FF-HEDM scan was taken to determine the residual state of the material.

HEDM is an X-ray technique that rotates a sample while it's illuminated by a monochromatic X-ray beam (61.332 keV), where the multiple modalities of HEDM can be used to reconstruct the morphology of the grains (Fig. 2b), along with the 3D grainaveraged lattice strain tensor for each grain in the illuminated region [15,20,21]. The HEDM characterization setup and associated resolutions are described in Gustafson et al. [22] and further in the supplemental material. As FF-HEDM captures, but does not differentiate, mechanical elastic strains and thermal strains, the exact temperatures of each loading state were determined by first subtracting the macroscopic elastic strains due to loading, then calculating the average hydrostatic strain from all of the grains within the 600  $\mu m$  tall scan volume, and finally determining the corresponding temperature by comparing to thermal expansion data [16]. The conversion from elastic strain to stress was completed with a scaling of the elastic moduli [23] based on Young's modulus as a function of temperature data [16]. The resolution of the

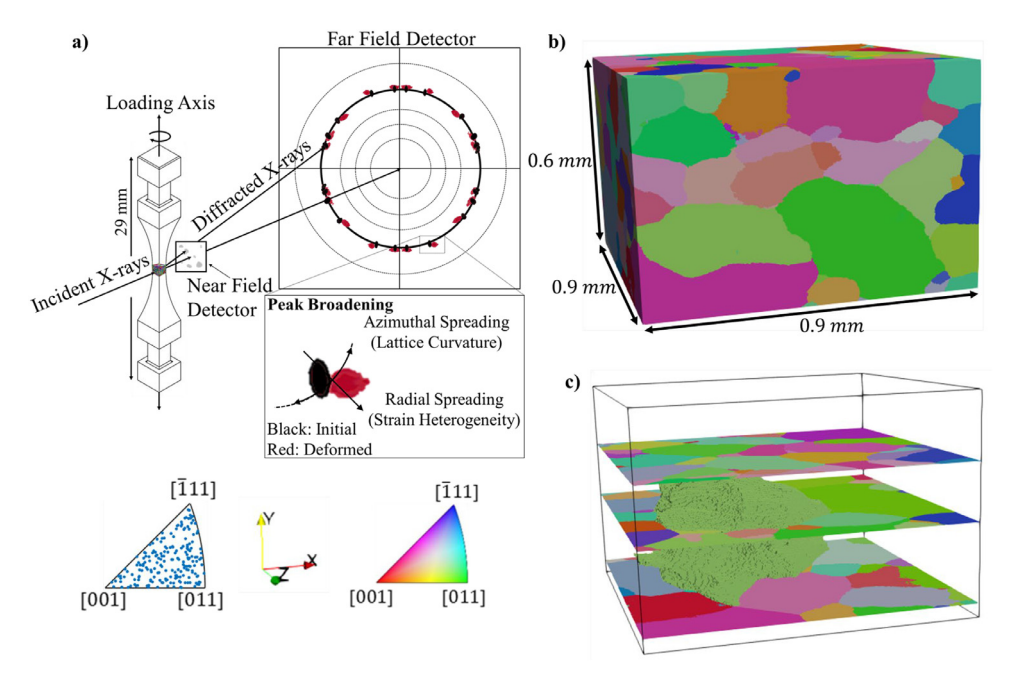


Fig. 2. (a) HEDM schematic with specimen design. Adapted with permission from [22]. (b) Reconstructed NF-HEDM volume colored by IPF. (c) Slices of reconstructed NF-HEDM with single large grain.

grain averaged orientations and elastic strains captured from FF-HEDM are noted to be better than  $0.05^{\circ}$  and  $10^{-4}$ , respectively (which leads to a 50 MPa resolution in the grain averaged stresses) [21,24]. While standard FF-HEDM analysis provides only grain averaged quantities, such as updated orientations and elastic strain information at every state, intragranular information can also be gleamed from further investigation of the FF-HEDM diffraction peaks via peak broadening analysis [25]. This technique, as illustrated in Fig. 2a, calculates the full width of the diffraction spots in the FF-HEDM data in the three polar coordinate directions ( $\eta$ ,  $\omega$ ,  $2\theta$ ), specifically  $\eta$  in this analysis. Each direction is associated with a particular lattice distortion feature within a single grain, and  $\eta$ spreads, as used in this work, can be determined with 0.06° resolution (based on the pixel size of the detector). Spread of diffraction spots in the  $\eta$  direction is associated with intragranular misorientation (lattice curvature) [26], while spread in the  $2\theta$  direction indicates intragranular elastic strain [26,27]. As  $\eta$  spread captures the extent of lattice curvature within a grain, which is associated with dislocation content, specifically geometrically necessary dislocations (GNDs) [28], it can be used as a metric to capture the relative amount of recovery within a grain (dislocation annihilation, rearrangement, and sub-grain formation). The full width of the diffraction spots was used in this work to capture all possible localized intragranular misorientations, existing in the fringes of the diffraction spots (often of lower intensities on the detector) and can subsequently be lost in metrics, such as the full width half max. The reconstructed data from NF-HEDM, FF-HEDM and peak broadening analysis were combined and post processed via a combination of an in-house Matlab script and a Dream3D pipeline, then visualized in ParaView.

The spatial region of interest (ROI) interrogated in the sample is shown in Fig. 2, b. and c. In particular, a large grain is captured in this ROI that is observed to be 4.5x greater than the average grain size of this sample. While the average grain diameter within this reconstruction is 92.84  $\mu m$ , the grain diameters range from 7  $\mu m$  to 453  $\mu m$  (see supplemental material for a histogram of the grain diameter distribution). Three slices of the full 3D NF-HEDM volume are placed above, bisecting the middle, and under the bulk of a large grain within the ROI, as shown in Fig. 2c; however,

conclusions in this study were drawn independently of grain size. This data presentation method displays that this single large grain, which has forty-eight neighboring grains, can experience gradients of stress states across its volume. By coloring each individual grain with a single value of a metric, such as stress or strain, Figs. 3 and 4 allow a simple spatial visualization of data and enable context to be gleamed from the surrounding grains for each of the seven states mentioned previously.

To understand the failure mechanisms active during TMF, the stress state and evolution must be tracked within the microstructure during loading. Fig. 3a displays grains from the NF-HEDM reconstruction colored with the stress in the loading direction, as calculated from FF-HEDM. Between states 1 and 7 the sample underwent relatively large amounts of plasticity, which changed the defect configuration within the grains and led to significant heterogeneity of the stresses between the two states. Grain scale residual stresses are observed post deformation in state 7, as illustrated by the large grain (indicated with arrows in Fig. 3a). Fig. 3a also shows that between states 1 and 2 there was a slight stress redistribution upon the initial heating due to the neighborhood interactions of grains with varying orientations during isotropic expansion. Fig. 3b shows the hydrostatic stress deviation from the mean hydrostatic stress to better display the heterogeneous stress distribution. The hydrostatic stresses show similar trends as the stress in the loading direction, with a redistribution between states 1 and 2 upon initial loading and a larger distribution in the final state as compared to the first. Fig. 3 highlights the heterogeneous stress evolution experienced by individual grains and underlines that interactions on the grain scale must be considered to fully investigate TMF.

Complementing the complex, grain scale stress evolutions, the resultant deformation of the grains are probed to better understand the mechanisms experienced during TMF loading. From peak broadening analysis and FF-HEDM, we are able to infer information about the intragranular and intergranular plastic deformation occurring in the microstructure during loading. Fig. 4a displays the change in the spread of  $\eta$ , a metric capturing the change in intragranular misorientation between the current state and prior state. While we measure the spread in  $\eta$ , which is due to lattice curvature, we will refer to it as lattice curvature for brevity and to mit-

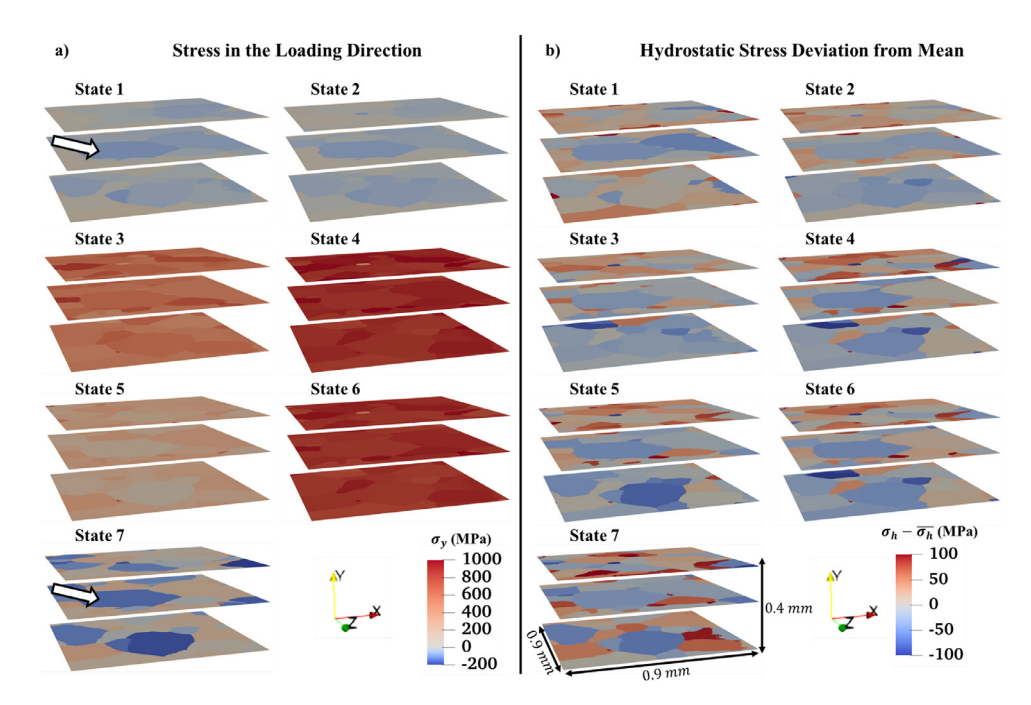


**Fig. 3.** (a) Slices of NF-HEDM colored with stresses in the loading direction  $(\sigma_y)$  with white arrows indicating a grain of interest in states 1 and 7. (b) Slices of NF-HEDM colored with the deviation of the hydrostatic stress from the mean hydrostatic stress  $(\sigma_h - \overline{\sigma_h})$ .

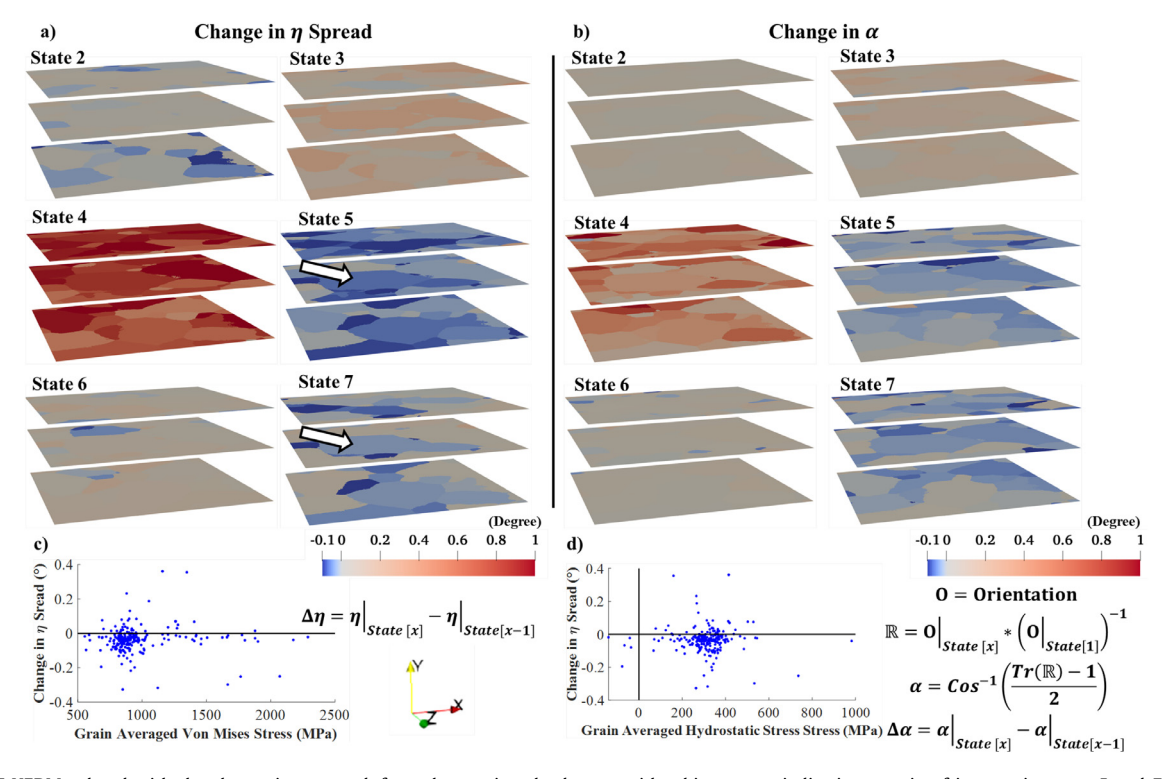


**Fig. 4.** (a) NF-HEDM colored with the change in  $\eta$  spread, from the previous load state, with white arrows indicating a grain of interest in states 5 and 7. (b) NF-HEDM colored with  $\Delta \alpha$ , the change in misorientation from the previous load state, such that each  $\alpha$  is the misorientation relative to state 1. (c) Change in  $\eta$  spread (state 5 – state 4) vs grain averaged von Mises stress (state 4). (d) Change in  $\eta$  spread (state 5 – state 4) vs grain averaged hydrostatic stress (state 4).

igate confusion with  $\alpha$  (grain averaged misorientation). In state 3, which is macroscopically near yielding of the material, the grains display a heterogeneous change to lattice curvature where not all of the grains have plasticized; likely the result of anisotropy. Fig. 4b displays  $\Delta\alpha$  which is the difference in misorientation angle between the current state and prior state; misorientation angle  $\alpha$  is calculated individually for each state relative to state 1 to allow for

 $\Delta \alpha$  to capture the signed change in misorientation angle. Similar to  $\eta$  spread, intergranular heterogeneity is observed in the misorientation angle evolution in state 3, indicating that some grains underwent a rigid body rotation (either elastic, plastic, or a combination) of the grains away from their initial states, while others have rotated back towards their original orientations. Grains at state 4, corresponding to the first drop in temperature, exhibited

the largest degree of plasticity with many of the grains rotating by nearly a degree (Fig. 4b) and the lattice curvature within many of the grains also increasing by a similar magnitude (Fig. 4a). Both states 5 and 7 indicate that dynamic recovery took place via a decrease in the lattice curvature and a reorientation back towards the original orientation; the rigid, grain-averaged reorientation back to the original configuration can be attributed to elastic unloading. The change in  $\eta$  spread shows similar results for both states 5 and 7, except that state 5 had a larger degree of recovery than state 7, as highlighted by the arrows demarcating the same large grain in Fig. 4a. Due to the elevated temperature, which has been shown to accelerate the dynamic recovery process, state 5 likely had both stages of recovery, dislocation rearrangement and sub-grain formation, as observed by Hasegawa and Kocks [10], while the dynamic recovery in state 7, which was near room temperature, would likely be a continuation of the unloading effects.

Dynamic recovery, as described by the change of the spread in  $\eta$ , represents a rearrangement (decrease in density) of the GNDs in the material and as such, an analysis was conducted to determine if the grain averaged stresses determinable by FF-HEDM influenced the recovery process. Notably, no correlation was found between the grain-scale stress state prior to dynamic recovery and the magnitude of recovery (nor if the grain would recovery at all) as shown in Fig. 4, c. and d. This indicates an inability of grain-scale stresses to accurately predict the amount of recovery likely for a particular grain and points to sub-grain scale factors such as local stress state, coarsening of  $\gamma'$  precipitate (rafting), and dislocation structures to play a role in the extent of recovery experienced by a single grain. It should be noted that during large amounts of plasticity, such as that seen in state 4, smaller grains will lose accuracy in their reconstruction allowing for stresses far above expected values as demonstrated in Fig. 4c. Additionally, investigations were completed to discover if a pseudo form of the stored strain energy, comprised of a stress term and a metric representing plastic strain (based on broadening of the diffraction spots in the  $\eta$  and  $2\theta$  directions), in state 4 gave indication to the amount of recovery seen for each grain in state 5. The investigations provided no evidence that the stored strain energy term described above was linked to the amount of recovery seen, which suggests that complex grain interactions, particularly those around large grains such as that shown in Fig. 2c with forty-eight neighboring grains, cannot easily be captured by the grain averaged metrics and therefore future work is needed to investigate a grain pair or cluster with higher spatial resolution to analyze the effects of lower-length scale defect structures. The investigation of the microstructural response, in-situ, is not only critical to study effects, such as the heterogeneous nature of dynamic recovery, but to study the many loading conditions experienced during TMF.

In summary, grain scale metrics were tracked during thermomechanical loading, providing a necessary first step to describe the role of the microstructure during TMF loading. X-ray techniques, such as HEDM, present the ability to investigate mechanisms occurring on the grain scale such as polycrystalline dynamic recovery. Additionally, as shown by Ahl et al. [13], X-ray experiments can provide sub-grain resolution to explore individual grains in greater detail during the recovery process. This study shows that the elevated temperatures experienced during TMF loading have the ability to reconfigure the substructure of a polycrystalline nickel-based superalloy into a new state after deformation. This reconfiguration can be detrimental in critical components as a reduction in flow stress can lead to a reduction in the fatigue performance of the material, and premature failure. It also illustrates that, as with most other microstructural fields such as stress and strain, the amount of recovery in a polycrystal is heterogeneous, yet grain scale metrics are inadequate to accurately predict the degree of recovery available to a specific grain. Additionally, this work provides the framework for explorations of both elastic and intragranular deformation metrics during full TMF loading and its resulting failure mechanisms.

#### **Author Contributions**

S.G. performed the HEDM experiment, reconstruction, and associated analysis and wrote the first draft of the manuscript. D.P. was the beamline scientist providing the set-up and expertise to perform the HEDM experiment and provided critical insight into the HEDM reconstructions. P.S. assisted the HEDM experiment and provided insight into the material characteristics. M.S. assisted the HEDM experiment, conceived the idea for this work, and supervised the research. All co-authors provided reviews of the manuscript.

# **Declaration of Competing Interest**

The authors declare that they have no known competing financial interests or personal relationships that could have appeared to influence the work reported in this paper.

# Acknowledgements

This work was supported by the National Science Foundation (grant number CMMI 16-51956) under program manager Dr. Alexis Lewis. In-situ high energy X-ray microscopy was performed at the Cornell High Energy Synchrotron Source (supported by the National Science Foundation under DMR-1829070), with beamline support provided by Dr. Peter Ko. The authors would like to thank Dr. Diwakar Naragani for the peak broadening analysis scripts, help with their implementation and adaption to the dataset of interest, and support during the beamtime. Additionally, the authors would like to thank Dr. Bill Musinski for providing material. P.S. acknowledges support from the Materials & Manufacturing Directorate and the Air Force Office of Scientific Research (program manager Jay Tiley) of the U.S. Air Force Research Laboratory.

## Supplementary materials

Supplementary material associated with this article can be found, in the online version, at doi:10.1016/j.scriptamat.2020.10.

# References

- [1] R.W. Neu, H. Sehitoglu, Metall. Trans. A 20 (1989) 1755-1767.
- [2] D.A. Boismier, H. Sehitoglu, J. Eng. Mater. Technol. 112 (1990) 68-79.
- [3] H. Sehitoglu, D.A. Boismier, J. Eng. Mater. Technol. 112 (1990) 80–89.[4] A. Pineau, S.D. Antolovich, Eng. Fail. Anal. 16 (2009) 2668–2697.
- [4] A. Pilleau, S.D. Alltolovich, Eng. Fall. Anal. 16 (2009) 2668–2697.[5] M.D. Sangid, H.J. Maier, H. Sehitoglu, J. Mech. Phys. Solids 59 (2011) 595–609.
- [6] W.D. Musinski, D.L. McDowell, Int. J. Fatigue 37 (2012) 41–53.
- [7] S.P. Bhat, C. Laird, Fatigue Fract. Eng. Mater. Struct. 1 (1979) 59–77.
- [8] D.L. Holt, J. Appl. Phys. 41 (1970) 3197-3201.
- [9] H. Mughrabi, Acta Metall. 31 (1983) 1367–1379.[10] T. Hasegawa, U.F. Kocks, Acta Metall. 27 (1979) 1705–1716.
- 11] T. Hasegawa, T. Yakou, U.F. Kocks, Acta Metall. 30 (1982) 235–243.
- [12] B. Jakobsen, H.F. Poulsen, U. Lienert, J. Almer, S.D. Shastri, H.O. Sørensen, C. Gundlach, W. Pantleon, Science (80-.) 312 (2006) 889–892.
- [13] S.R. Ahl, H. Simons, C. Detlefs, D.J. Jensen, H.F. Poulsen, Acta Mater. 185 (2020) 142–148.
- [14] J.C. Schuren, P.A. Shade, J.V. Bernier, S.F. Li, B. Blank, J. Lind, P. Kenesei, U. Lienert, R.M. Suter, T.J. Turner, D.M. Dimiduk, J. Almer, Curr. Opin. Solid State Mater. Sci. 19 (2015) 235–244.
- [15] D.C. Pagan, J.V. Bernier, D. Dale, J.Y.P. Ko, T.J. Turner, B. Blank, P.A. Shade, Scr. Mater. 142 (2018) 96–100.
- [16] T.P. Gabb, J. Gayda, J. Telesman, P.T. Kantzos, (2005) 82.
- [17] W.D. Musinski, P.A. Shade, D.C. Pagan, J. V. Bernier, Prep. (n.d.).
- [18] P.A. Shade, B. Blank, J.C. Schuren, T.J. Turner, P. Kenesei, K. Goetze, R.M. Suter, J.V. Bernier, S.F. Li, J. Lind, U. Lienert, J. Almer, Rev. Sci. Instrum. 86 (2015) 093902.
- [19] S.F. Li, R.M. Suter, J. Appl. Crystallogr. 46 (2013) 512-524.

- [20] H. Poulsen, Three-Dimensional X-Ray Diffraction Microscopy, Springer Berlin Heidelberg, Berlin, Heidelberg, 2004.
  [21] J.V. Bernier, N.R. Barton, U. Lienert, M.P. Miller, J. Strain Anal. Eng. Des. 46
- [21] J.v. Berniet, N.R. Baiton, U. Lienert, M.P. Miller, J. Strain Anal. Eng. Des. 46 (2011) 527–547.
  [22] S. Gustafson, W. Ludwig, P. Shade, D. Naragani, D. Pagan, P. Cook, C. Yildirim, C. Detlefs, M.D. Sangid, Nat. Commun. 11 (2020) 3189.
  [23] A. Cerrone, C. Stein, R. Pokharel, C. Hefferan, J. Lind, H. Tucker, R. Suter, A. Rollett, A. Interfere Model. Signal, March Sci. Eng. 20 (2015) 2015005.
- lett, A. Ingraffea, Model. Simul. Mater. Sci. Eng. 23 (2015) 035006.
- [24] R.C. Hurley, E.B. Herbold, D.C. Pagan, J. Appl. Crystallogr. 51 (2018) 1021–1034.[25] D.P. Naragani, P.A. Shade, P. Kenesei, H. Sharma, M.D. Sangid, Acta Mater. 179 (2019) 342–359.
- [26] M. Obstalecki, S.L. Wong, P.R. Dawson, M.P. Miller, Acta Mater. 75 (2014) 259-272.
- [27] J. Oddershede, J.P. Wright, A. Beaudoin, G. Winther, Acta Mater. 85 (2015) 301–313.
- [28] M.F. Ashby, Philos. Mag. A J. Theor. Exp. Appl. Phys. 21 (1970) 399-424.